Ceramics International 51 (2025) 59777–59788

Contents lists available at ScienceDirect

Ceramics International

journal homepage: www.elsevier.com/locate/ceramint

Room temperature preparation of Ti_2AlC MAX-phase films using the powder aerosol deposition method

Andrea Groß, Daniel Paulus, Till Scholz, Ralf Moos *, Daniela Schönauer-Kamin

Department of Functional Materials, University of Bayreuth, 95447 Bayreuth, Germany

ARTICLE INFO

Handling Editor: P. Vincenzini

Keywords:
Powder aerosol deposition (PAD)
MAX-phase Ti_2AlC
A. Films
B. Grain size

ABSTRACT

The MAX-phase Ti_2AlC is interesting as a temperature-stable electrical contact material and, due to the formation of a protective alumina scale on the surface, also as an oxidation-resistant and self-healing coating. For the first time, the powder aerosol deposition method (PADM) is applied to prepare homogenous Ti_2AlC-films directly from the raw powder at room temperature. Besides the material's microstructure, initial tests address the thermal stability and the electrical resistivity of PADM-Ti_2AlC. µm-sized Ti_2AlC-particles are deposited as adhesive, up to 20 µm thick and dense Ti_2AlC-films on electrically insulating alumina or turbine-relevant titanium aluminides. The PADM-Ti_2AlC films with an average roughness of about 1 µm exhibit a nanocrystalline microstructure and retain the phase composition of the applied powder. Initial results on the thermal stability of PADM-Ti_2AlC in air up to 800 °C are promising: The film-integrity is preserved and light discolorations as well as slight film growth indicate oxide formation at the surface. Moderate thermal annealing of PADM-films is known to relax microstrain that origins from the high-energy particle impact and limits electrical conductivity. Accordingly, the resistivity of PADM-Ti_2AlC is reduced by 68 % after annealing at 800 °C in nitrogen atmosphere. The final value of 6.8 µΩm of the nanocrystalline PADM-films is one order of magnitude above those of common thin-films. Electrical measurements as well as SEM images indicate the formation of surficial oxide during heat treatment in air.

1. Introduction

MAX-phases advantageously combine ceramic and metallic properties. Additionally, Al-containing MAX-phases like titanium aluminum carbide Ti_2AlC form passivating oxides. Therefore, temperature-resistant, mechanically stable, and electrically conductive Ti_2AlC-films have great potential as electrical contacts [1–11] and protective coatings for thermally highly stressed components [2,5,11–13]. Intermetallic titanium aluminide (γ-TiAl), for example, offers superior specific strength up to 900 °C [14–16], but its application in turbines is limited by embrittlement due to fast-growing oxides above 700 °C [12]. MAX-phase coatings have the potential to significantly enhance the applicability of γ-TiAl in turbine environments by improving oxidation resistance and mitigating embrittlement. However, the large-scale deposition of well-adhering, uniform, and thick MAX-phase coatings of high purity is challenging [11,17–19]. As a proof-of-principle, we report for the first time that several µm thick, dense, and electrically conductive Ti_2AlC-films can be prepared directly from the powder at room temperature by the powder aerosol deposition method (PADM). The unique nanocrystalline and deformed microstructure of PADM-films will promote the understanding of the structure-property relationships of Ti_2AlC, which is mandatory for an application-oriented design.

2. Theory

MAX-phases ($M_{n+1}AX_n$) are layered ternary carbides or nitrides with an early transition-metal (M, like titanium Ti), an A-group element (A, mainly aluminum Al, or silicon Si) and carbon or nitrogen (X). The hexagonal close-packed (hcp) crystal structure comprises edge-shared M_6X-octahedra interleaved with pure metallic close-packed A-layers. While the M-X bonding is strongly ionic-covalent, the weaker M-A metallic bonding provides some chemical activity as well as shear deformability in the basal plane [3,4,8,11,19–27]. The low electrical resistivity is dominated by the transition-metal and increases linearly with temperature [2,6,10,23,24,28–32]. Room temperature values of bulk-Ti_2AlC range from 0.2 to 0.5 µΩm [3,6,8,28,30–33], while thin films exhibit 0.4 to 1.0 µΩm [7,9,28,34,35]. Charge carrier scattering at lattice defects [2] due to non-stochiometric material compositions [32],

* Corresponding author.
E-mail address: functional.materials@uni-bayreuth.de (R. Moos).

https://doi.org/10.1016/j.ceramint.2025.10.205
Received 4 July 2025; Received in revised form 23 September 2025; Accepted 14 October 2025
Available online 15 October 2025

fine grains [8,35] and microstrain [36] impairs conductivity. Thermally grown oxides (TGO) can provide oxidation resistance and self-healing of Al-containing MAX-phases [2–4,11–13,21,22,25,37–46]. Diffusion of weakly bound Al-atoms along the basal plane at elevated temperatures enables the growth of a few μm thick layer of aluminum oxide (α-Al_2O_3) at the surface, which inhibits inward diffusion of oxygen and outwards diffusion of titanium. The competitive formation of α-Al_2O_3 and non-passivating rutile (TiO_2) on Ti_2AlC is influenced by the microstructure, since fine grains accelerate the growth of a protective scale [2,42–44,47,48]. Crucial for a protective scale is a temperature of at least 700 °C [42], better 800 °C [39,41,49], as well as a high purity of the MAX-phase [39,42,50]. Defects and surface roughness promote TiO_2--formation and lower the adhesion of TGOs [8,43,51,52].

Physical vapor deposition (PVD) is suitable for high-crystalline thin Ti_2AlC-films [1,4,11,12,23,26,35]. Thick films are prepared by thermal spraying, but the high temperatures required for partial melting of the powder cause destructive tensile stresses, material degeneration, and oxidation [11,26,41,53,54]. Contrarily, conventional kinetic spray techniques like cold spray (CS) base on plastic deformability upon high-energetic ballistic impingement at low temperatures [8,19,55] and retain the phase composition as well as the crystallographic structures of the applied powder [8,11,17–19,26,53,55–58]. Residual compressive stress enhances the integrity and the mechanical strength of CS-films [18], but large stress causes inter-splat delamination and poor adhesion [19,53,55,57,58]. Hence, there is a continuing need for low-temperature processes for several μm thick polycrystalline MAX-phase coatings on technologically relevant substrates [4,26]. The fast, versatile, and low-cost powder aerosol deposition method (PADM) might satisfy this demand.

PADM is suitable to deposit additive-free, dense, nanocrystalline, and several μm thick ceramic or metallic films from the powder at room temperature on a variety of materials [59–66]. This vacuum-based kinetic spray coating method is also denoted as aerosol deposition method (AD or ADM) [59,66–68], vacuum kinetic spraying [64], or vacuum cold spraying [58]. It requires no additional interlayer, no specific gas precursors and no thermal energy for ablation, vaporization, or chemical reactions. Sub-μm to μm-sized particles are accelerated in the dry powder aerosol to several hundred m/s and directed to the substrate. Depending on the hardness, impinging particles plastically deform the surface of the substrate, and a firmly adhering anchor layer forms [69,70]. Film growth bases on room temperature impact consolidation (RTIC) [59–61,63,65,70–73]: Hitting the substrate, a part of the kinetic energy of the particles is converted into shear deformation and fracture energy. The deformed fragments are compacted by subsequent impacting particles (hammering effect) and form a dense polycrystalline film. Besides the mechanical properties, the velocity, the size, and the morphology of the powders are decisive for uniform, adhering and dense coatings [59,60,69]. PADM-films are known to exhibit a nanocrystalline morphology with high defect densities, atomic lattice deformations (microstrain) and film-immanent compressive stresses, all affecting their mechanical and electrical properties [62,65,73–77]. Since the PADM requires no heat treatment for film formation, the phase composition is retained and can be adjusted by the applied powder [63,72,78]. However, moderate thermal annealing far below the sintering temperature can relax residual strains and thereby enhance the electrical conductivity of the deformed microstructure [65,74,76,79].

Recently, nano-structuring has been recommended to enhance the oxidation resistance and adhesion of MAX-phase coatings [44]. The unique nanocrystalline morphology of PADM-films might elucidate the required structure-property relationships of MAX-phases [11,13,44]. However, to the best of our knowledge, the PADM has not yet been applied for MAX-phases except for Ti_3SiC_2 [66–68,78]. Due to deviations in the mechanical properties, the results on PADM-Ti_3SiC_2 cannot be easily transferred to other MAX-phases. Herein, the PADM was applied for the first time to deposit Ti_2AlC on electrically insulating alumina, intermetallic γ-TiAl and Si-wafers. Initial results on the morphology, the thermal stability as well as the electrical conductivity of PADM-Ti_2AlC are depicted. Since no thermal energy is required for phase formation during deposition, the thermal post-treatment of PADM-Ti_2AlC-films could be focused on structural relaxation and/or surface passivation by TGOs.

3. Material and methods

3.1. Materials and powder milling

Purchased titanium aluminum carbide (Ti_2AlC) MAX-phase micron powder (99 % purity of the elements, 325 mesh, Nanografi Nano Technology, Cankaya Ankara, Turkey) was ground in a planetary ball mill (Pulverisette 5, Fritsch GmbH, Idar-Oberstein, Germany) with 200 ml cyclohexane as dispersion media and 50 WC/Co milling balls with a diameter of 10 mm in the WC/Co milling jar. The process consisted of 21 cycles of 5 min of milling, and 25 min pauses to avoid heating of the powder. Therefore, the Ti_2AlC-powder was milled for a total of 105 min at 400 rpm. Afterwards, the dispersion media was removed by a rotary evaporator. The powder was dried at 120 °C, sieved with a 90 μm mesh to avoid agglomerates that impair the aerosol generation and stored in nitrogen atmosphere until deposition.

3.2. Film deposition

Using a custom-made powder aerosol deposition apparatus, Ti_2AlC-films were deposited at room temperature on 630 μm thick alumina substrates (96 % Al_2O_3, Rubalit 708 S, CeramTec, Plochingen, Germany), 3.5 mm thick cuts of titanium aluminide γ-TiAl samples (TiAl48-2-2, GfE Metalle und Materialien GmbH) and 50 μm thick silicon wafer cuts with (9 1 1) orientation (CrysTec Kristalltechnologie, Berlin, Germany) for XRD-analysis. No chemical or thermal treatment of the substrates prior to the deposition was required.

The powder aerosol deposition apparatus depicted in Fig. 1 consists of an aerosol generator and a deposition chamber evacuated by a vacuum pump. The PADM operates at room temperature and neither the powder nor the substrate are heated. First, the powder aerosol was generated in a fluidized bed by mixing a few grams of the grounded Ti_2AlC-powder in a bottle on a vibrating table (400–720 min^{-1}) with a continuous nitrogen carrier gas flow of 6–10 l/min. Then, the pressure gradient between the aerosol generator and the deposition chamber accelerates the powder aerosol through a convergent slit nozzle (10 x 0,5 mm^2) towards the substrate (2 mm substrate-nozzle distance). Impacting the substrate surface, the powder particles are deposited due to the RTIC-mechanism and form a dense, nanocrystalline ceramic film. For areal coatings, the substrates can be moved by a programmable stage with a speed of 5 mm/s. The thickness of the Ti_2AlC-films can be varied by passing the substrate between 40 and 300 times.

3.3. Characterization methods

The morphology of the milled Ti_2AlC-powder was investigated by scanning electron microscopy (SEM, Zeiss Leo 1530, Oberkochen, Germany). The particle size distribution of the milled Ti_2AlC-powder was compared to those of the as-received one via laser diffraction (Mastersizer 2000, Malvern Instruments Ltd, Malvern, United Kingdom).

The film-quality was evaluated optically by light microscopy (BX60M, Olympus, Hamburg, Germany). The microstructure of the as-deposited Ti_2AlC-films at the top-view as well as the un-polished and polished cross-section was analyzed by SEM (Zeiss Leo Gemini 1530 VP, Oberkochen, Germany). Film thickness and roughness were determined using a perthometer (Waveline W20, Jenoptik AG, Jena, Germany) with a diamond stylus tip (2 μm/90°) and a cutoff wavelength of 0.8 mm. Depending on the dimensions of the coated area, the profiles were evaluated over a length of 4–10 mm. Additionally, on selected samples the roughness was confirmed with a 3D laser-scanning-microscope (LSM

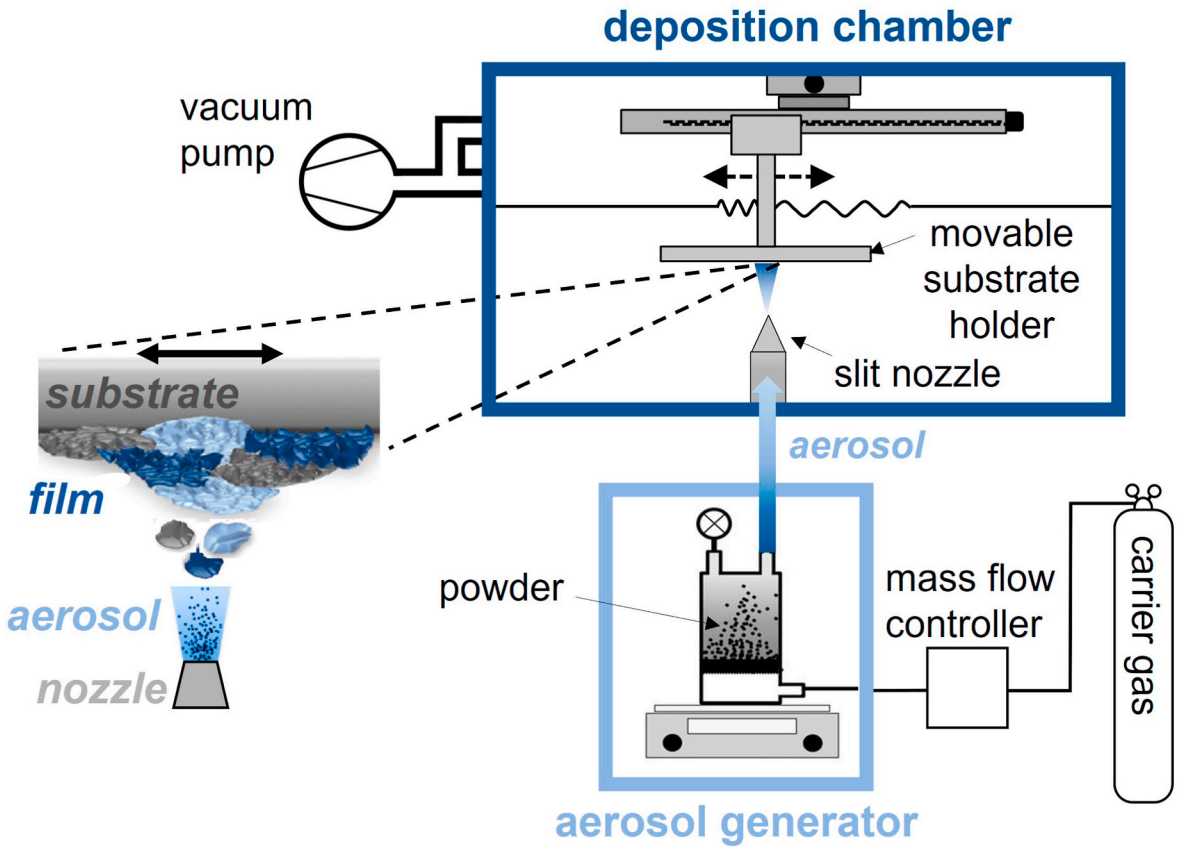

Fig. 1. Schematic overview of the powder aerosol deposition apparatus with a slit nozzle directing the accelerated powder from the aerosol generator to the movable substrate holder in the deposition chamber.

900M, Carl-Zeiss AG). This proof-of-principle-study does not include a statistical evaluation of the roughness.

X-ray diffraction (XRD) analysis in a Bragg-Brentano arrangement (Bruker D8 Advance, Bruker GmbH, Karlsruhe, Germany) with Cu-K_α radiation with Ge (1 1 1) primary beam monochromator ($\lambda = 1.5418$ Å) and a Lynxeye 1D detector served to compare the crystalline phase composition of the powder before and after milling to those of PADM-Ti_2AlC-films on silicon wafers. The diffraction patterns were recorded at room temperature in a 2θ range between 10° and 80° with a point distance of 0.02° and a recording time of 10 s per step.

To investigate the thermal stability of powder aerosol deposited Ti_2AlC-films, the samples were treated at defined temperatures from 300 to 800 °C in a custom-built gas flushable furnace with a diameter of the tube of about 30 mm. The gas flows of pure nitrogen or synthetic air (20 % O_2 and 80 % N_2) at a flow rate of at least 200 ml/min were adjusted with mass flow controllers. A zirconia-based potentiometric oxygen sensor ensured a timely constant oxygen concentration. A thermocouple next to the PADM-Ti_2AlC-sample was used to measure and control the temperature. In the gas-purged tube furnace, the samples were heated with a heating rate of 10 K/min, treated for 1 h or 3 h at the intended temperature and cooled in the gas flowing to room temperature by switching off the heater.

The electrical resistivity ρ_{RT} of the PADM-Ti_2AlC-films on alumina substrates was determined in ambient air at room temperature and related to the previous heat-treatment. Therefore, the top-surface of the film was electrically contacted by a four-point probe head (SP4, 302 Lucas/Signatone Corporation, USA) with a spacing between the tips of 1016 µm, a tip radius of 254 µm and a spring pressure of 45 g. The DC-resistance R was determined from the voltage measured with a Keithley 2400 Source Meter at an applied current of 1–10 mA. ρ_{RT} was calculated from R and the thickness of the film d_{film} according to the theory of a thin extended film with a corresponding correction factor to account for the geometry.

4. Results

In the following, the suitability of the PADM for the deposition of Ti_2AlC on alumina and intermetallic γ-TiAl is demonstrated and initial results on the electrical resistivity as well as the oxidation resistance of PADM-Ti_2AlC are shown.

4.1. Powder pre-treatment

For the film growth by RTIC, the kinetic energy of the particles, and thus their inertia, must be high enough for them to fracture and compact on impact [59,61]. However, large particles lead to erosion or cannot be transferred to the powder aerosol in the first place [59,61]. Hence, a suitable pre-treatment of the powder to be deposited by the PADM is essential for film formation [60]. According to the particle size distribution in Fig. 2, by milling the mean particle size d_{50} was reduced from about 13.2 µm to 5.4 µm compared to the as-received Ti_2AlC-powder. The span between the percentile values d_{10} and d_{90} was diminished from 30.1 µm to 14.7 µm and the relative span related to the mean value amounts to 2.3 for the as-received and 2.7 for the milled powder. Hence, most of the milled particles are in the appropriate range for the RTIC-mechanism to receive adhering films [61].

According to the XRD-measurement in Fig. 3 and in agreement with [80], the as-received technical Ti_2AlC-powder (black line) is not phase-pure. It contains at least significant amounts of Ti_3AlC_2 and most probably other Ti-Al-compositions and carbides such as TiC. However, despite long analysis times and Bragg-Brentano corrections, it was not possible to reliably resolve the strongly overlapping reflections of the

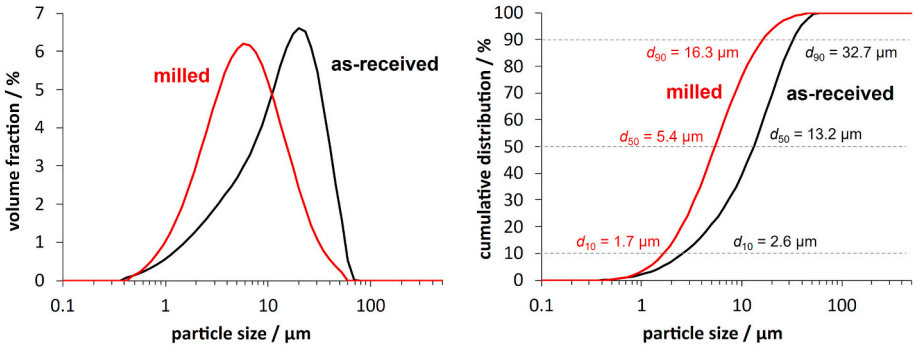

Fig. 2. Particle size distribution of the milled (red) and the as-received Ti_2AlC-powder (black): a) differential distribution and b) cumulative distribution. (For interpretation of the references to color in this figure legend, the reader is referred to the Web version of this article.)

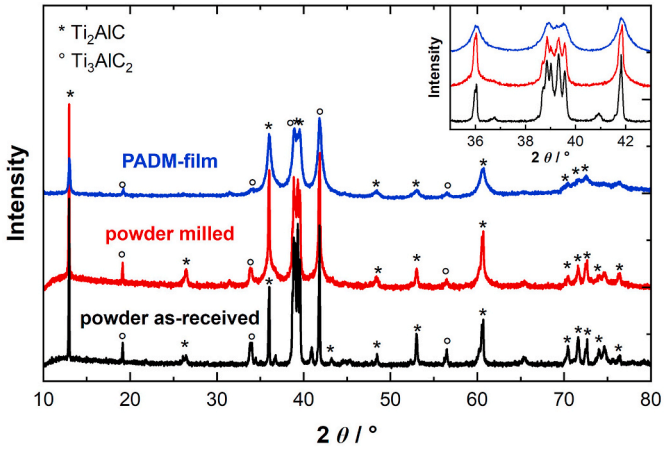

Fig. 3. XRD-pattern of the milled (red) and the as-received Ti_2AlC-powder (black) compared to those of a PADM-Ti_2AlC-film on silicon (blue). Reference positions of Ti_2AlC (04-021-3073) and Ti_3AlC_2 (04-012-0632) reflections are indicated. (For interpretation of the references to color in this figure legend, the reader is referred to the Web version of this article.)

powder. The existence of various phases in combination with the present anisotropic strain, which strongly broadens parts of the reflections, prevents a reliable model for a quantitative Rietveld refinement. However, the comparison of the XRD-patterns of the as-received (black line) and the milled powder (red line) reveals that milling largely retains the phase composition. In addition to the reduced crystallite size, the slightly higher breadth of the reflections might origin from an increase in the microstrain of the crystal lattice due to the mechanical stress introduced in the planetary ball mill.

The SEM micrographs of the milled powder in Fig. 4 show irregularly shaped particles of diverse sizes with sharp edges (a). Lamellar patterns at the surface of the Ti_2AlC-grains reveal the distinctive layered, terrace-like structure of the nano-laminated MAX-phase (b). Presumably due to the mechanical stress during milling, the laminate seems to be deformed, and the particles are mainly, but not exclusively, fractured along the basal planes leading to delamination and cleavage. At some particles, fine flakes seem to adhere to the surface of coarser particles resulting in conglomerates (c).

4.2. Film deposition

By the PADM, the milled Ti_2AlC-powders can be successfully deposited at room temperature as continuous, about 10–20 µm thick and well-adhering films on alumina, γ-TiAl and silicon. The integrity of the films is maintained even when the surfaces are manually scratched with a knife blade, demonstrating the high scratch resistance of PADM-Ti_2AlC-films. Fig. 5a shows an image of a dark-brown PADM-Ti_2AlC-film uniformly covering the white alumina substrate. The upper right corner that had been broken off for SEM demonstrates good film adhesion. The two light optical micrographs at different magnifications in Fig. 5b confirm that a homogeneous coating with a certain surface unevenness was achieved. By perthometer and LSM, the roughness of various Ti_2AlC-films on alumina substrates was determined to range from 0.9 to 1 µm. No dependency of R_a on the direction relative to the spray path was found. Hence, the PAD-Ti_2AlC-films are rougher than the applied Rubalit 708S alumina substrates, whose surface roughness is specified in the data sheet as $R_a \leq 0.6$ µm. Exemplarily, Fig. 5c depicts the profile stylus of a 11.6 µm thick and about 8.5 mm broad Ti_2AlC-stripe on alumina. The roughness of the surface of PADM-Ti_2AlC was determined from the profile over the evaluation length from 1.5 to 9 mm to be R_a = 0.94 µm (center line average) and R_z = 6.60 µm.

Despite the polished γ-TiAl-cuts provide a smoother surface with $R_a \approx 0.06$ µm than the applied alumina substrates, Ti_2AlC could be

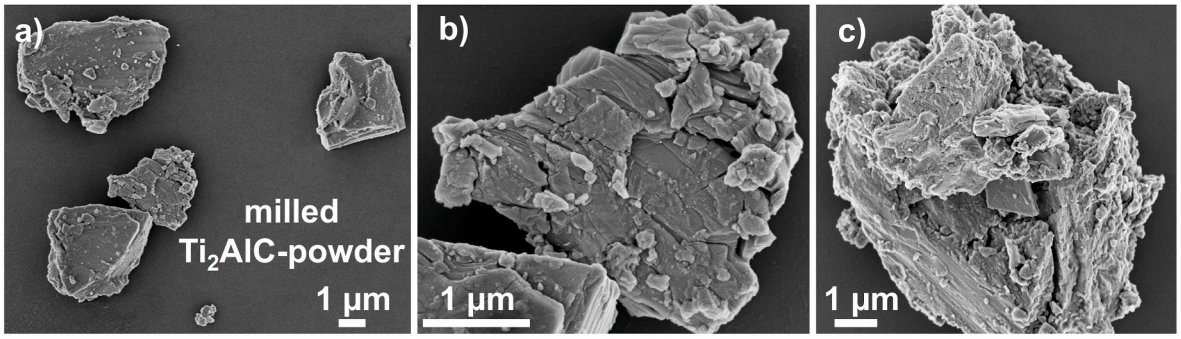

Fig. 4. SEM images of the milled Ti_2AlC-powder in different magnifications: a) particles in diverse sizes, b) partly deformed and fractured multilayer structure and c) adherent flakes.

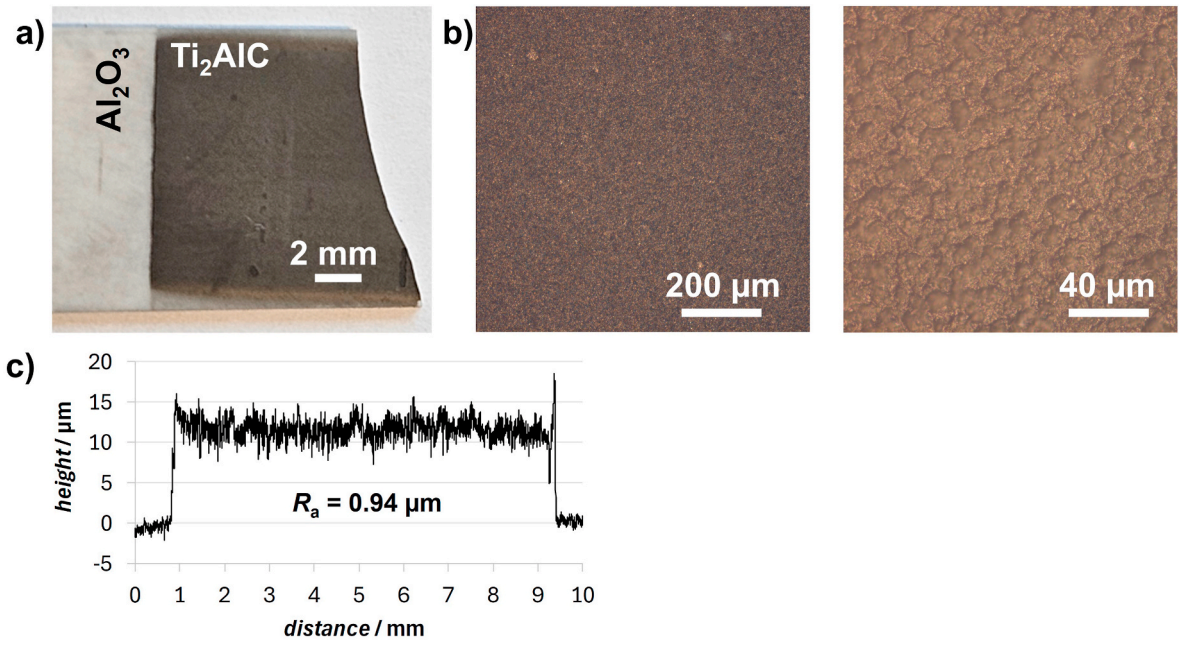

Fig. 5. As-deposited PADM-Ti_2AlC-films on alumina substrates: a) surface of a sample with a break edge for SEM, b) light optical microscope images of the surface in two magnifications, c) surface profile of a 11.6 µm thick and about 8.5 mm broad Ti_2AlC-film.

deposited with the same PADM-parameters. Fig. 6a depicts the homogeneous dark-brown surface of an 8 mm × 5 mm sized PADM-Ti_2AlC-coating. On γ-TiAl, the 17 µm–20 µm thick PADM-Ti_2AlC-films exhibit R_a-values of about 1.7 µm–1.8 µm. Exemplarily Fig. 6b depicts a 19.2 µm thick and about 5 mm broad film with a roughness R_a = 1.76 µm (evaluated over the length from 1.0 to 5.0 mm). The higher thickness and roughness of PADM-Ti_2AlC on γ-TiAl compared to alumina might be caused by differences in the hardness and the surface quality of the applied substrates. As summarized in Refs. [69,81], smoother ceramic substrates increase the deposition rate of alumina and more ductile substrates reduce the fragmentation of impacting particles but enhance the anchoring layer.

The unchanged position of the reflections in the XRD-pattern of the PADM-Ti_2AlC-film on silicon compared to the milled powder in Fig. 3 clarifies that the film deposition by the PADM generally preserves the crystal structure of the applied Ti_2AlC-powder. No significant phase degradation or oxidation of the applied material due to the deposition at room temperature can be detected by XRD. However, a detailed comparison reveals a pronounced broadening of the reflections, and a reduced intensity compared to the milled powder. This indicates either the decrease of crystallite size due to size broadening, an increase of microstrain associated with microstrain broadening, or both. The decrease of the intensity is a direct consequence of reflection broadening. This result is typical for PADM-films and can be attributed to the RTIC-mechanism: Fragmentation and deformation cause a reduction in the crystallite size and an increase in microstrain of the crystal lattice [60,61]. In accordance, upon powder aerosol deposition of Ti_3SiC_2 also no new crystalline phases were found, but the crystallites got smaller and residual microstrain occurred [68,78]. Deviations in the relative reflection intensities of the PADM-film from the milled powder indicate a texture of the deposited and compacted particles.

The morphology and the adhesive interface of the Ti_2AlC-film on alumina in the as-deposited state were further studied by SEM of the fracture surface of the sample depicted in Fig. 5a. Fig. 7a displays the cross-section of the Ti_2AlC-sample at the unpolished fracture edge. The 17.7 µm thick Ti_2AlC-film seems to be uniform, non-porous, and free of delamination, voids, or cracks. Hence, the integrity of the PADM-Ti_2AlC-films on alumina is maintained even when the coated substrates are broken, indicating a stable adhesion between the deformed particles as well as to the substrate. Typically for aerosol deposited films, the microstructure consists of small fragments. The nanocrystalline structure of PADM-films originates from the high-energetic impact leading to fragmentation and compaction of the particles (RTIC-mechanism). In the magnification of the broken edge, the fracture surface appears uneven and rough. This might be attributed to the high fracture toughness of MAX-phases resulting in pull-outs and crack deflection upon breaking the sample [32]. There seems to be no clear orientation of the nano-laminated grains. The top-view of the Ti_2AlC-film in Fig. 7b confirms a crack-free and non-porous microstructure consisting of splats that form a rough surface due to grain refinement.

This initial proof-of-principle demonstrates the suitability of the PADM for the deposition of Ti_2AlC with particles in the size of a few µm

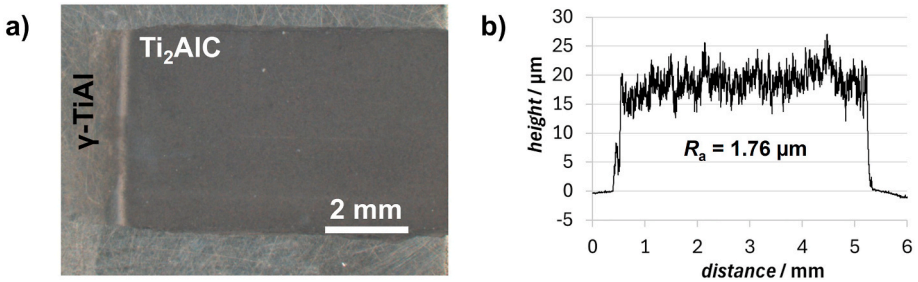

Fig. 6. As-deposited PADM-Ti_2AlC-films on γ-TiAl: a) image of the surface, b) surface profile of a 19.2 µm thick and 5 mm broad Ti_2AlC-film.

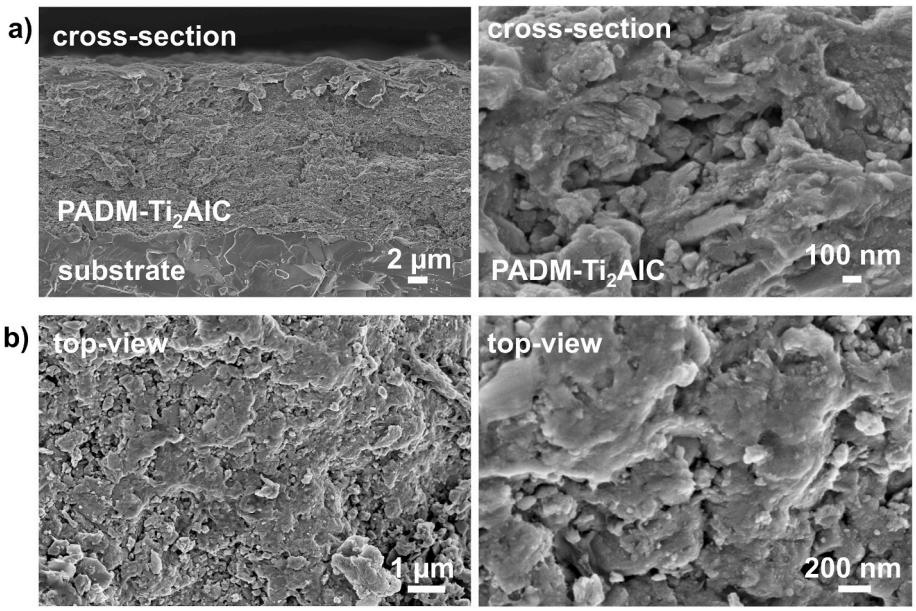

Fig. 7. SEM images of the as-deposited PADM-Ti_2AlC-film on alumina substrates in different magnifications: a) fractured cross-section, b) top-view onto the surface.

at room temperature on alumina and γ-TiAl. However, detailed, and quantified investigations on the adhesion, the density, the morphology, the surface quality as well as the phase composition and the microstructure of PADM-Ti_2AlC in dependency on experimental parameters as well as the applied substrate are open for further studies.

4.3. Electrical resistivity

The electrical resistivity at room temperature ρ_{RT} of PADM-Ti_2AlC was determined on substrates of electrical insulating alumina. ρ_{RT} was calculated from the sheet resistance measured non-destructively with a four-point probe head at the surface of the film and the determined film thickness. ρ_{RT} of as-deposited PADM-Ti_2AlC-films is about 20 µΩm. Hence, it is almost two decades above reported values of 0.5–0.7 µΩm for conventional Ti_2AlC-thin-films produced by PVD [35,82]. However, this is a reasonable result, since the charge carrier mobility of PADM-films is known to be reduced by the nanocrystalline microstructure as well as the high defect density [65,83,84].

In the past, microstrain of nanocrystalline PADM-films that reduce the electrical conductivity was relaxed without grain growth by moderate thermal post-treatment [65,74,76,79]. To study the effect of thermal annealing on the electrical resistivity of PADM-Ti_2AlC, the coated alumina substrate shown in Fig. 5a was stored at increasing temperatures $T_{annealing}$ from 440 to 800 °C for 1 h each. Thereby, the tube furnace was continuously flushed with nitrogen to avoid oxidation of Ti_2AlC. In between the individual temperature steps, the sample was cooled to room temperature to determine ρ_{RT} under ambient gas conditions outside the furnace. Thereby, changes of the film surface due to annealing could be monitored optically. The micrographs of the surface in Fig. 8a under non-identical light conditions depict that the PADM-Ti_2AlC-film remained mechanically intact during this thermal treatment. However, starting from about 700 °C in nitrogen, white discolorations appeared. The light optical microscope magnifications of the annealed surface in Fig. 8b confirm finely distributed light spots and light crusts at uneven areas as well as the edges of the film. In consideration of the anisotropic chemical activity of Ti_2AlC, these discolorations must be addressed by a highly resolved chemical analysis in the future. The course of ρ_{RT} as a function of $T_{annealing}$ in Fig. 8c reveals that annealing up to 800 °C decreases the resistivity of the Ti_2AlC-film from 21.1 µΩm to 6.8 µΩm. The biggest change in resistivity appears between 500 °C and 700 °C. Although ρ_{RT} of PADM-Ti_2AlC was reduced thermally by almost 70 %, the final value of 6.8 µΩm is still one decade above literature data on the resistivity of PVD-films [35,82]. Future research needs to address the origin of the enhanced resistivity of

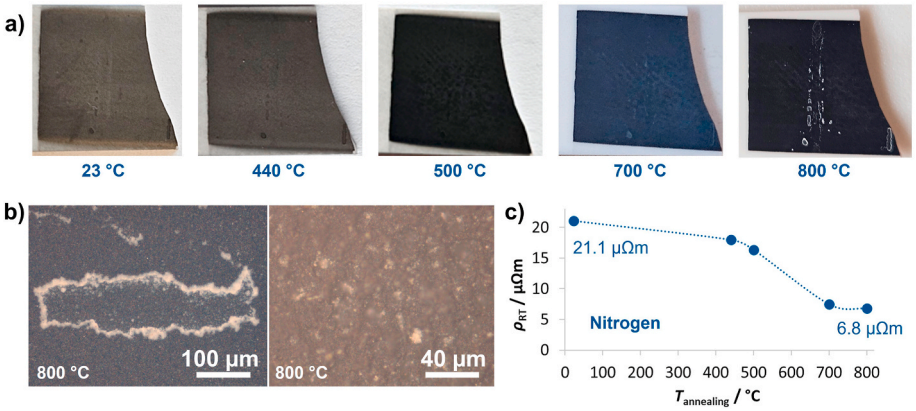

Fig. 8. Effect of proceeding annealing of PADM-Ti_2AlC in nitrogen for *1 h at various temperatures* $T_{annealing}$*: a) micrographs of the surface dependent on* $T_{annealing}$*, b) magnifications of discolored areas after 800 °C, c) resistivity at room temperature* ρ_{RT} *as a function of* $T_{annealing}$.

PADM-Ti_2AlC compared to PVD-films considering deviations in the microstructure, but also the influence of secondary phases.

4.4. Heat treatment in air

Since Al_2O_3 is electrically insulating and TiO_2 is a semiconductor, TGO-formation is expected to decrease the electrical conductivity at least at the surface of the Ti_2AlC-film [9,35]. To study the effect of an oxidizing environment on the resistivity of the PADM-Ti_2AlC-films, the thermal treatment of the same sample was repeated in synthetic air for 1 h at 300 °C and 1 h at 800 °C. The visual nature of the coating, the thickness of the Ti_2AlC-film d_{film} and its electrical resistivity ρ_{RT} were studied under ambient conditions at room temperature in between the heating steps.

As can be seen from Fig. 9a, storing the sample 1 h at 300 °C in air only negligibly affects the appearance of the coating. However, 1 h at 800 °C results in a white top layer on the Ti_2AlC-film indicating a chemical reaction under oxidizing conditions. In Fig. 9b, the resistivity ρ_{RT} and the thickness of the Ti_2AlC-film d_{film} are correlated with the maximum temperature of the previous heat treatment $T_{treatment}$. ρ_{RT} and d_{film} are only slightly affected by 300 °C. The values increase from 6.8 µΩm to 7.0 µΩm and from 17.7 µm to 17.8 µm, respectively. However, treating the film for 1 h at 800 °C in air, the thickness increased by more than 7 % from 17.7 µm to about 19 µm indicating oxidation. In accordance with the assumption of oxide formation, no electrical contact to the surface of PADM-Ti_2AlC could be established by the four-point probe tips after heat treatment at 800 °C, which prevented the measurement of the final value of the resistivity. Fig. 9c depicts the polished cross-section of a 22.8 µm thick PADM-Ti_2AlC-coating that was kept for 1 h at 800 °C in synthetic air. The SEM images at two different magnifications confirm that the annealed and probably oxidized film is dense and well interlocked with the alumina substrate. The absence of delamination or cracks into the depths of the film, at the interface to the substrate and at the gas-exposed surface demonstrates the temperature-stability of PADM-Ti_2AlC-films on alumina up to at least 800 °C. In accordance with the optical appearance of the surface in Fig. 9a, the cross section shows a thin top layer that could represent an oxide layer.

To investigate the influence of the duration of a thermal treatment in air at 800 °C $t_{800\,°C}$, the sample that had already been treated for 1 h was broken into two pieces and one half was kept for another 2 h at 800 °C. As shown in Fig. 10, due to the extended treatment for 3 h at 800 °C, the film grew to about 20 µm without losing its mechanical integrity or the adhesion to the substrate. This is an increase in d_{film} of approx. 13 % related to the thickness of 17.7 µm prior to heating. Fig. 10b compares light optical microscope images of the surface of the PADM-Ti_2AlC-coating after 1 h (left) and 3 h (right) in air at 800 °C. After 1 h, white spots appeared at the surface especially in uneven areas and at the edges of the film. After 3 h, however, a homogeneous, white-colored, and furry layer covers continuously the entire film. This material transformation might be caused by proceeding surficial oxide formation. No spalling of parts of the film itself or the white crust was observed upon this thermal treatment. In accordance, the thermally grown protective scale of Ti_2AlC-coatings is known to have a suitable thermal expansion coefficient and a certain ductility that supports integrity during thermal cycling and improves the tribological as well as mechanical properties [4,5,8,12,37–40,44,49,51].

5. Discussion and outlook

The PADM promises mechanically stable as well as oxidation-resistant nanocrystalline MAX-phase coatings on high-temperature sensible components. In the past, it has only been applied to the MAX-phase Ti_3SiC_2 [66–68,78]. Here, Ti_2AlC was deposited by the PADM for the first time. To place these very initial results in a larger scientific context, they are related to the well-known characteristic properties of powder aerosol deposited films and Ti_2AlC in the following. By now, the role of non-quantified secondary phases of the applied technical powder on the powder deposition as well as on the mechanical, electrical, or protective properties of PADM-Ti_2AlC cannot be evaluated. Further research priorities arise also from the observation of a diminished resistivity of PADM-Ti_2AlC compared to PVD-films and of discolorations upon heating.

5.1. Morphology and phase composition

While the dual ceramic-metallic character of MAX-phases makes cold spraying (CS) challenging [19], herein the suitability of the PADM-technology to deposit several µm thick, well-adhering, and homogenous Ti_2AlC-films directly from technical Ti_2AlC-powder on alumina as well as application-relevant γ-TiAl alloy-substrates (48-2-2TiAl) was demonstrated. The applicability of the PADM for MAX-phase coatings is confirmed, and the soft metal layers of the specific MAX-phase crystal structure seem not to hinder bonding [66]. The applied aerosol velocity is sufficiently high to fracture and compact the impacting Ti_2AlC-particles at room temperature on various substrate materials. In the future, however, variations in powder pretreatment, including the particle size and a defined pre-heat-treatment could enhance the deposition efficiency as well as the properties of the coating [60].

Material degradations of Ti_2AlC are well-known disadvantages of film depositions at high temperatures [26,53,54], but can be avoided by low temperature processes such as CS [17,19,53,55–57]. In accordance,

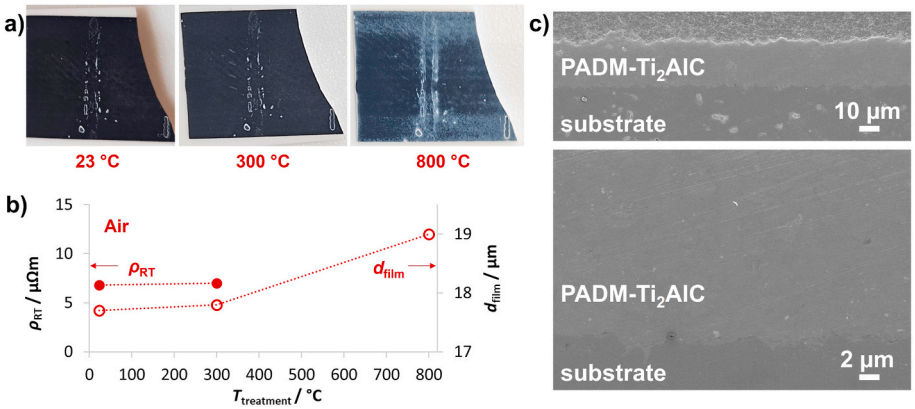

Fig. 9. Effect of proceeding thermal treatment of PADM-Ti_2AlC in synthetic air for 1 h at 300 °C and 800 °C: a) micrographs of the surface, b) room temperature resistivity ρ_{RT} *and film thickness* d_{film} *as a function of the annealing temperature* $T_{treatment}$, *c) SEM of a polished cross-section of a* 22 µm *thick PADM-*Ti_2AlC*-film on alumina treated for 1 h at 800 °C in synthetic air in two different magnifications.*

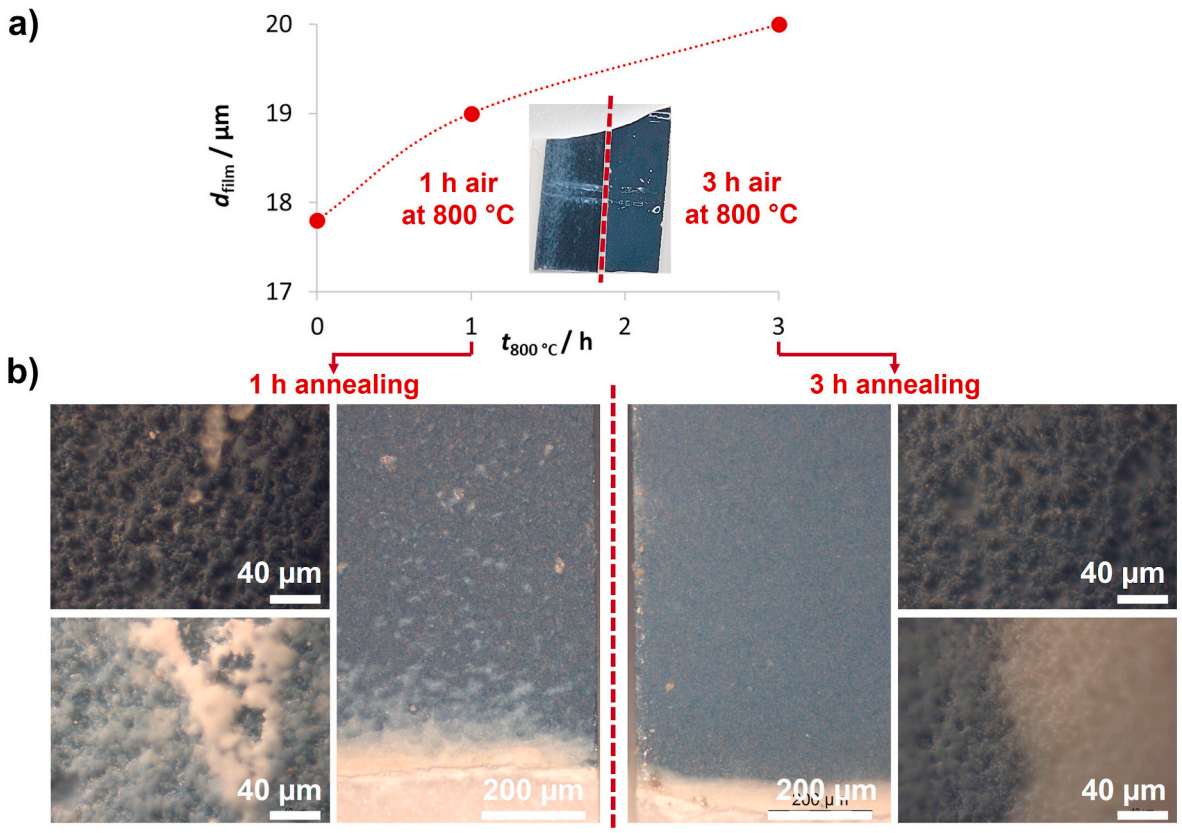

Fig. 10. Effect of the duration of the heat treatment at 800 °C in air on PADM-Ti_2AlC-films on alumina: a) film thickness d_{film} *as a function of duration* $t_{800\,°C}$ *and b) light microscopy images of 1h and 3h heat treated coatings.*

the comparison of XRD-data of the applied Ti_2AlC-powder and the therefrom obtained PADM-Ti_2AlC-films also do not indicate significant phase changes: neither milling of the as-received powder nor subsequent powder aerosol deposition at room temperature changed the phase composition of the raw Ti_2AlC material in a significant way. In consequence, powder aerosol deposition enables the adjustment of the material composition of the Ti_2AlC-film by an appropriate powder selection.

The XRD-data also clarifies that the used starting powder is not phase-pure. Like in other "technical" Ti_2AlC [56,85], reflections of phases like Ti_3AlC_2 and TiC predominantly overlap and decrease the reliability of a Rietveld refinement. Despite long analysis times and the necessary Bragg-Brentano corrections, the available XRD device could not reliably resolve the strongly overlapping reflections of the Ti_2AlC--powder or the PADM-Ti_2AlC-film. In addition, the reflex broadening of mechanically stressed powders and PAD-films prevented the quantitative determination of the phases, crystallite sizes and microstrain. From these initial results, the influence of secondary phases on the powder deposition as well as the resulting properties of PADM-Ti_2AlC-films cannot be estimated. Future studies need to address the quantification of the phase composition as well as of the microstructure.

The surface roughness is important for the high-temperature stability of Ti_2AlC-films since it is known to affect the oxidation behavior: On the one hand, a rough surface enhances the adhesion at the Ti_2AlC-TGO-interface, especially upon thermal cycling [52]. On the other hand, rough coatings promote spalling during oxidation [43] and TiO_2--formation [43,52,86]. Destructive rumpling of the TGO is reported to occur if the roughness exceeds 3 µm [51]. Independent on the direction relative to the spray path, the center line average of the surface roughness of Ti_2AlC on alumina and γ-TiAl is about 0.9 and 1.8 µm, respectively. For comparison, a roughness of 300 nm was reported for 10 µm PADM-Ti_3SiC_2 on glass [78], which could be attributed in deviations in the mechanical properties. Of course, the PADM generates rougher films than PVD (nm-range [24]). However, the Ti_2AlC-surfaces obtained by powder aerosol deposition are smoother than those produced by other spray technologies: Markocsan et al. [53] obtained a roughness R_a of 8 µm with high velocity air fuel spraying, 6 µm with high velocity oxygen fuel spraying, and 5 µm by CS of Ti_2AlC, whereas Loganathan et al. [17] report on 2.4 µm for CS-Ti_2AlC. According to the determined roughness, PADM-Ti_2AlC-films are smoother than other sprayed films and hence, they might have a superior resistance to oxidation.

While CS-Ti_2AlC-films are reported to be affected by voids or cracks [17,53,55–57], SEM of a broken and a polished cross-section of PADM-Ti_2AlC reveals a dense microstructure which is attributed to the RTIC deposition mechanism.

Mechanical stresses during milling and due to the high-energy impact for the RTIC-mechanism are known to fracture crystals and induce defects in the crystals in PADM-films [60,61]. In fact, the nanocrystalline microstructure of PADM-Ti_2AlC causes a broadening of the XRD-reflections. Reflection broadening has also been reported for PADM-Ti_3SiC_2 [68,78] and CS-Ti_2AlC [19,53,56,57]. Unfortunately, the strong overlapping of the broadened reflections in combination with an unknown phase composition prevents a reliable quantitative analysis of the microstrain and the mean crystallite size by Rietveld refinement. Changes in the relative intensities of the reflections indicate some texturing of the powder aerosol deposited Ti_2AlC-films. In the future, the existence of a preferred orientation of the deposited particles as well as a quantification of the crystallite size and the microstrain in dependency of the film thickness and the applied substrate could be addressed by depositing a Ti_2AlC-powder with a high purity of the desired phase. A spatially resolved analysis of the microstructure by transmission electron microscopy might further shed light on the arrangement of the nanolayered Ti_2AlC-grains in the powder aerosol deposited film and at the interface.

5.2. Thermal stability and oxidation

Ti_2AlC is investigated as high-temperature stable and oxidation resistant coating, since it can form a protective α-Al_2O_3-scale at the surface [2–4,11,12,21,22,25,37–43]. In this initial study, the thermal stability of PADM-Ti_2AlC was addressed by heating a film on an alumina substrate stepwise to 800 °C in nitrogen and air. Thereby, the integrity of the film was completely preserved demonstrating the strong interface between the alumina substrate and the PADM-Ti_2AlC. Discolorations on the surface and a slight thickness increase indicate chemical reactions upon thermal treatment in both gas atmospheres. Light spots on the surface of the PADM-Ti_2AlC-films initially appear in uneven areas and at edges of the coating before spreading equally over the entire surface.

By now, an analysis of the evolved reaction products at the surface of the deposited Ti_2AlC-films and their occurrence in the depths of the film is pending. However, the optical findings on PADM-Ti_2AlC are consistent with the reported thermal stability of Ti_2AlC, which is known to depend on gas atmosphere, as well as sample geometry and morphology [39,52,87,88]: Calculations on the thermochemical stability at 700 °C in pure nitrogen predict the formation of aluminum nitride AlN, titanium nitride TiN and residual carbon [87]. At low oxygen content, non-stoichiometric titanium carbide $TiC_{0.5}$ and aluminum nitride AlN with small fractions of Al_2O_3 are expected [87]. Hence, the observed color change from dark-brown to dark-grey after heating the PADM-Ti_2AlC--films in nitrogen (containing traces of oxygen) might be an indicator for the surficial formation of dark-grey TiC_x. The light borders of uneven areas might origin from the evolution of white AlN and yellow TiN. In the future, elemental mapping of the cross-section of heat-treated samples is intended to provide spatially resolved information about phase evolution as a function of the gas atmosphere.

While sintered Ti_2AlC-compacts maintain their structure in argon up to at least 800 °C, decomposition in air is known to begin at 447 °C [88]. According to the calculated thermochemical stability, the oxides Al_2O_3 and TiO_2 form at 700 °C in air and pure oxygen [87]. In fact, upon heating in air, the color at the surface of PADM-Ti_2AlC-films turned light-grey with white spots indicating oxide formation. Similarly, a change from dark-grey to light-grey above 400 °C was also reported on Ti_2AlC-powders [85]. In particular, the powder color after oxidation at 800 °C in Ref. [85] strongly resembles that of the PADM-Ti_2AlC-film treated at the same temperature in air, also indicating the surficial formation of α-Al_2O_3 and rutile TiO_2 on PADM-Ti_2AlC-films. Furthermore, the observed increase in thickness upon heating in air is in accordance with the reported volume expansion of the powder upon oxidation [85]. To prevent destruction of the PADM-Ti_2AlC sample, unusually high volume expansions at temperatures around 600 °C [8,10,49,85] were avoided. Commercially available powders usually contain mixtures of Ti_2AlC and Ti_3AlC_2, intermetallic Ti_xAl_y and TiC [50,85]. Those secondary phases are expected to influence the oxidation behavior. Although the oxidation mechanism is similar, Ti_2AlC oxidizes faster than Ti_3AlC_2 due to the higher Al-content [25,38]. Impurities like Ti_xAl_y and TiC are known to be preferentially oxidized without forming a protective scale [41,42,50] and at a lower temperature [85]. In further studies, thermogravimetric analysis as well as differential scanning calorimetry on the applied powder will give further insights into the temperature dependent oxidation kinetics and phase transformations.

As summarized in Ref. [44], the surface roughness, the grain size, the texture as well as residual stress influence the reaction kinetics of oxide formation, the competition between passivating α-Al_2O_3 and non-passivating TiO_2 as well as the mechanical stability of the protective scale. Therefore, besides the chemical composition of the applied powder, the unique morphology must also be considered when studying thermal stability of PADM-films. The nanolayered crystal structure of Ti_2AlC is known to cause anisotropic chemical activity: Owing to the low formation energy for Al-vacancies, Al-atoms diffuse thermally activated along the basal planes, accumulate on the outer surface perpendicular to the nanolayers, and react with the gas atmosphere [3,22,25,37,39,41]. As a result, fine-grained Ti_2AlC is reported to shift the onset-temperature of oxidation from 400 °C to 300 °C [47]. Hence, considering the nano-crystallinity of PADM-coatings, the high readiness to react with the gas atmosphere is not surprising. Contrary to PVD-films, by now there is no hint for a pronounced texturing PADM-Ti_2AlC with an alignment of the basal planes. As already discussed, the surface roughness of 0.9 and 1.8 μm seems appropriate to restrict TiO_2-formation [43,52,86] and to promote the adhesion of the TGO [43,51,52].

For all these reasons, it is expected that upon thermal treatment of PADM-Ti_2AlC, nitrides and oxides are formed, beginning from the gas-exposed surface. It is hypothesized that the dense, low-textured, and nanocrystalline microstructure in combination with the uniform surface promotes the growth and stability of a protective α-Al_2O_3-scale by an accelerated and equal out-diffusion of aluminum. The well-interlocked interface between the powder aerosol deposited film and the TGO is intended to elevate oxidation resistance additionally. According to the self-healing properties of Ti_2AlC [2,13,38,44–46] even an increase in the mechanical strength of the coating by closing microscale interspaces by TGOs is conceivable.

In the future, the deposition of Ti_2AlC-powders with a high purity in combination with a detailed analysis of the chemical composition of heat-treated surfaces using high-resolution XRD or IR spectroscopy could clarify the evolution of nitrides and oxides to better assess the high-temperature performance of PADM-Ti_2AlC. To evaluate the potential of the powder aerosol deposition technology for protective MAX-phase-films, further research on the mechanical and high temperature properties of PADM-Ti_2AlC-films on γ-TiAl is required.

5.3. Influences on electrical resistivity

The Ti-containing MAX-phases Ti_2AlC, Ti_3AlC_2, and Ti_2AlN are known for their high electrical conductivity along the basal planes [3,6,8,10,28–33,89,90]. Depending on the film preparation, the resistivity of Ti_2AlC-thin-films is about 0.4–1.0 μΩm [7,9,28,34,35]. Besides phase-impurities [10,32,90], defects, scattering of electrons and microstrain deforming the crystal lattice might increase the electrical resistivity of Ti_2AlC [36]. According to the data presented and further measurements conducted in the four-wire configuration, the room temperature resistivity of as-deposited Ti_2AlC-films ranges reproducibly from about 15 to 20 μΩm. Thus, the electrical resistivity of the prepared PADM-Ti_2AlC is almost two decades above those of thin-films generated by PVD.

Due to the nanocrystalline and deformed crystal structure, PADM-films usually exhibit a high defect density with microstrain affecting the electrical properties [62,65,73–77]. Hence, the reduced conductivity of PADM-Ti_2AlC can be explained by a reduced charge carrier mobility in the deformed nanocrystalline microstructure [65,83,84]. Commonly, residual stresses of PADM-films can be relaxed by a moderate thermal annealing preserving the crystallite size [65,74,76,79]. According to the relationship between annealing temperature and melting point given in Ref. [74], 800 °C should be a suitable temperature to relax powder aerosol deposited Ti_2AlC, which melts incongruently at 1625 °C [91]. In fact, upon thermally annealing the room temperature resistivity could be reduced by 68 % and the greatest improvement was observed in the range of 600 °C. These initial results demonstrate the possibility of thermally enhancing the conductivity of PADM-Ti_2AlC. However, the present data does not allow for a correlation of the resistivity with the microstrain or the crystallite size. Further research needs to be conducted to quantify the effect of thermal annealing on the microstructure and on the electrical resistivity of PADM-Ti_2AlC.

Although the resistivity was reduced by thermal post-treatment, the final value of the resistivities is still one decade above literature values of PVD-films [35,82]. Besides the already discussed phase impurities of the applied powder and the nanocrystalline microstructure of the deposited film, the diminished conductivity might also origin from chemical reactions with the gas atmosphere containing nitrogen with traces of

oxygen [87]. The intention of heating PADM-Ti_2AlC-films in nitrogen was to investigate the effect of thermal post-treatment separately from oxidation. However, there is a risk of chemical reactions with the gas atmosphere at least at the film surface. The assumption of newly formed chemical components is supported by local discolorations on the surface. Nitrogen penetration at 600 °C was reported to lead to the formation of highly conductive $Ti_2AlC_{0.5}N_{0.5}$ [7,9], whereas oxide formation would increase the resistivity [9,35]. Surficial TGO leaves non-stoichiometric $Ti_2Al_{1-x}C$ behind [39] and Al-vacancies are known to reduce the conductivity slightly [31]. Oxygen can also replace surficial carbon and form $Ti_2Al(C_{1-x}O_x)$, which enhances the number of electrons [92]. Calculations reveal that nitrogen or oxygen impurity atoms in the Ti_2AlC-lattice lower the formation energy of Al-vacancies, which is related to the growth of electrically insulating AlN or Al_2O_3 [93]. Furthermore, it has been reported that at 800 °C in argon, low protective θ-Al_2O_3 and TiN forms, which in turn oxidize easily to non-conductive TiO_2 [12].

Besides surficial oxide formation, the self-healing capability of Ti_2AlC [45] also needs to be considered. TGO formation to close micro-gaps between the deposited and deformed particles in PADM--Ti_2AlC would result in electrical insulating oxides deep into Ti_2AlC-film. The filling of cracks with TiC at low oxygen partial pressures [46] would reduce the conductivity as well [10,31,33,90].

To investigate the effect of oxidizing conditions on the resistivity, the thermal treatment was repeated in air. For the discussion of the oxidation behavior, impurities of the applied Ti_2AlC-powder as well as the unique microstructure of PADM-films need to be considered as well. The rapid formation of surficial electrically insulating phases upon heating to 800 °C prevents an analysis of the resistivity in air by four-point probe tips at the surface of the film. Since fine-grained Ti_2AlC was observed to oxidize already at 300 °C [47], chemical reactions of the nanocrystalline PADM-Ti_2AlC seem possible even at low temperatures. Due to lack of protective Al_2O_3-formation, anomalous high oxidation rates at about 600 °C are known to destroy Ti_2AlC-samples [41,51,85]. An incubation time of 0.5 h for oxygen to diffuse and to break the bonds is reported [48]. In the experiments conducted, the integrity of the powder aerosol deposited Ti_2AlC-film could be preserved by passing this temperature region quickly.

In the future, an analysis of the temperature-dependent phase composition at least on the surface will help to identify chemical reactions that might affect the electrical properties. In addition, thermal treatment in an inert gas atmosphere such as argon is recommended to prevent reactions between Ti_2AlC and nitrogen.

A deeper understanding of the effect of the unique microstructure on oxidation is mandatory to access the potential of the PADM for Ti_2AlC as high temperature protective coatings. In future studies, highly phase-pure Ti_2AlC-powder should be applied to exclude influences of other phases. Additionally, a more frequent determination of the electrical properties upon thermal treatment in inert and oxidizing gas atmospheres are required. Monitoring the resistivity *in-situ* during heating by coated electrical transducers would be even more accurate. Of course, the electrical measurements need to be combined with a timely and spatially-resolved analysis of the chemical reactions at the surface and in the depths of the powder aerosol deposited film.

6. Conclusions

Ti_2AlC offers great potential as high-temperature-stable coatings but requires low-temperature coating technologies for several µm thick and well-adhering films. First results on the powder aerosol deposition of Ti_2AlC are promising: milled Ti_2AlC-powder can be deposited at room temperature as well-adhering, homogeneous, 20 µm thick and dense coatings on alumina substrates and, moreover, also on application-relevant γ-TiAl alloy.

The PADM-Ti_2AlC-films were analyzed regarding their microstructure and their electrical resistivity as well as their thermal stability. The initial results were discussed against the background of the properties of the MAX-phase Ti_2AlC and of powder aerosol deposited films. Powder aerosol deposited Ti_2AlC exhibits a nanocrystalline microstructure and retains the phase composition of the raw powder. Beneficially, the films are smoother than those produced with conventional spraying technologies. They withstand thermal treatment up to 800 °C in nitrogen and air, but discolorations on the surface as well as an increased thickness indicate surficial chemical reactions, particularly in air. Exceeding 300 °C in air, an electrically insulating layer forms rapidly at the gas-exposed surface, which is supposed to be thermally grown oxide. The resistivity of as-deposited PADM-Ti_2AlC ranges from 15 to 20 µΩm. Moderate thermal annealing is known to relax microstrain that origins from the high-energy impact of the PADM and restricts electrical conduction. Although the resistivity could be reduced thermally by 68 % to 6.8 µΩm, the resistivity is still one order of magnitude above those of thin films prepared by PVD. The reason might be the remaining nanocrystalline microstructure of PADM-Ti_2AlC.

These initial findings also raise questions on the relationship between the nanocrystalline and deformed microstructure and the electrical resistivity as well as the oxidation resistance of Ti_2AlC. Essential for further investigations is a spatially and timely resolved analysis of the microstructure and the chemical composition into the depth of the PADM-Ti_2AlC-films in parallel to a more detailed electrical characterization under various conditions.

CRediT authorship contribution statement

Andrea Groß: Writing – original draft, Visualization, Project administration, Investigation, Formal analysis, Conceptualization. **Daniel Paulus:** Writing – review & editing, Resources, Investigation, Formal analysis. **Till Scholz:** Writing – review & editing, Validation, Resources. **Ralf Moos:** Writing – review & editing, Supervision, Data curation. **Daniela Schönauer-Kamin:** Writing – review & editing, Visualization, Supervision, Investigation, Formal analysis, Conceptualization.

Data statement

Data will be made available on request.

Statement

During the preparation of this work the authors used DeepL Write to improve the readability and language of the manuscript. After using this tool, the authors reviewed and edited the content as needed and take full responsibility for the content of the published article.

Funding sources

This research did not receive any specific grant from funding agencies in the public, commercial, or not-for-profit sectors.

Declaration of competing interest

The authors declare that they have no known competing financial interests or personal relationships that could have appeared to influence the work reported in this paper.

Acknowledgments

From the university of Bayreuth the authors would like to thank the Chair of Applied Mechanics and Fluid Mechanics (J. Sesterhenn) for the particle size distribution measurements, the Bavarian Polymer Institute (BPI, Keylab Electron and Optical Microscopy) for providing the SEM and the Department of Metals and Alloys (U. Glatzel) for providing the XRD device. Further thanks go to Mathias Galetz and Katharina Beck

(DECHEMA) for providing TiAl-substrates and for the fruitful discussion concerning further joint research activities on passivating PADM-Ti_2AlC.

References

[1] N. Abbas, X. Qin, S. Ali, G. Zhu, J. Lu, F.e. Alam, A.G. Wattoo, X. Zeng, K. Gu, J. Tang, Direct deposition of extremely low interface-contact-resistant Ti_2AlC MAX-phase coating on stainless-steel by mid-frequency magnetron sputtering method, J. Eur. Ceram. Soc. 40 (2020) 3338–3342, https://doi.org/10.1016/j.jeurceramsoc.2020.02.033.

[2] M.S. Alam, M.A. Chowdhury, T. Khandaker, M.S. Hossain, M.S. Islam, M.M. Islam, M.K. Hasan, Advancements in MAX phase materials: structure, properties, and novel applications, RSC Adv. 14 (2024) 26995–27041, https://doi.org/10.1039/d4ra03714f.

[3] L. Fu, W. Xia, MAX phases as nanolaminate materials: Chemical composition, microstructure, synthesis, properties, and applications, Adv. Eng. Mater. 23 (2021), https://doi.org/10.1002/adem.202001191.

[4] E.N. Reshetnyak, A.S. Kuprin, T.A. Prikhna, M.A. Bortnitskaya, V.A. Belous, Synthesis, structure and protective properties of PVD MAX phase coatings. A review. Part II. Structure, properties, application prospects, Probl. Atom. Sci. Tech. (2024) 76–95, https://doi.org/10.46813/2024-150-076.

[5] O. Berger, The correlation between structure, multifunctional properties and application of PVD MAX phase coatings. Part III. Multifunctional applications, Surf. Eng. 36 (2020) 303–325, https://doi.org/10.1080/02670844.2019.1656861.

[6] V. Mauchamp, W. Yu, L. Gence, L. Piraux, T. Cabioch, V. Gauthier, P. Eklund, S. Dubois, Anisotropy of the resistivity and charge-carrier sign in nanolaminated Ti_2AlC: experiment and ab initio calculations, Phys. Rev. B 87 (2013) 235105, https://doi.org/10.1103/PhysRevB.87.235105.

[7] V. Podhurska, O. Kuprin, T. Prikhna, O. Ostash, D. Pohl, M. Karpets, V. Sverdun, T. Serbeniuk, R. Chepil, P. Potapov, et al., Development of oxidation-resistant and electrically conductive coating of Ti-Al-C system for the lightweight interconnects of solid oxide fuel cells, Heliyon 10 (2024) e23275, https://doi.org/10.1016/j.heliyon.2023.e23275.

[8] J. Gonzalez-Julian, Processing of MAX phases: from synthesis to applications, J. Am. Ceram. Soc. 104 (2021) 659–690, https://doi.org/10.1111/jace.17544.

[9] T.A. Prikhna, O.P. Ostash, A.S. Kuprin, V. Podhurska, T.B. Serbenyuk, E. S. Gevorkyan, M. Rucki, W. Zurowski, W. Kucharczyk, V.B. Sverdun, et al., A new MAX phases-based electroconductive coating for high-temperature oxidizing environment, Compos. Struct. 277 (2021) 114649, https://doi.org/10.1016/j.compstruct.2021.114649.

[10] X.H. Wang, Y.C. Zhou, Layered machinable and electrically conductive Ti_2AlC and Ti_3AlC_2 ceramics: a review, J. Mater. Sci. Technol. 26 (2010) 385–416, https://doi.org/10.1016/S1005-0302(10)60064-3.

[11] G. Ma, A. Zhang, Z. Wang, K. Wang, J. Zhang, K. Xu, Y. Xu, S. Zhou, A. Wang, MAX phase coatings: synthesis, protective performance, and functional characteristics, Mater. Horiz. 12 (2025) 1689–1710, https://doi.org/10.1039/d4mh01001a.

[12] N. Laska, R. Swadźba, P. Nellessen, O. Helle, R. Anton, Oxidation behavior of Ti_2AlC MAX phase-based coating on a γ-TiAl alloy TiAl48-2-2 produced by DC magnetron sputtering, Surf. Coating. Technol. 480 (2024) 130601, https://doi.org/10.1016/j.surfcoat.2024.130601.

[13] M. Suh, D.H. Lee, W.G. Sloof, K.S. Lee, Effect of temperature on the healing capacity and mechanical properties of Ti_2AlC MAX phase ceramics, Int. J. Appl. Ceram. Technol. 21 (2024) 2757–2770, https://doi.org/10.1111/ijac.14704.

[14] B.P. Bewlay, S. Nag, A. Suzuki, M.J. Weimer, TiAl alloys in commercial aircraft engines, Mater. A. T. High. Temp. 33 (2016) 549–559, https://doi.org/10.1080/09603409.2016.1183068.

[15] H. Clemens, S. Mayer, Intermetallic titanium aluminides in aerospace applications – processing, microstructure and properties, Mater. High Temp. 33 (2016) 560–570, https://doi.org/10.1080/09603409.2016.1163792.

[16] J. Lapin, TiAl-based alloys: present status and future perspectives, in: Conference Proceedings of Metal 2009, 2009.

[17] A. Loganathan, A. Sahu, C. Rudolf, C. Zhang, S. Rengifo, T. Laha, B. Boesl, A. Agarwal, Multi-scale tribological and nanomechanical behavior of cold sprayed Ti_2AlC MAX phase coating, Surf. Coating. Technol. 334 (2018) 384–393, https://doi.org/10.1016/j.surfcoat.2017.11.067.

[18] W. Zhang, S. Li, X. Zhang, X. Chen, Research and development on cold-sprayed MAX phase coatings, Coatings 13 (2023) 869, https://doi.org/10.3390/coatings13050869.

[19] A. Ion, P. Sallot, V. Badea, P. Duport, C. Popescu, A. Denoirjean, The dual character of MAX phase nano-layered structure highlighted by supersonic particles deposition, Coatings 11 (2021) 1038, https://doi.org/10.3390/coatings11091038.

[20] M.W. Barsoum, M. Radovic, Elastic and mechanical properties of the MAX phases, Annu. Rev. Mater. Res. 41 (2011) 195–227, https://doi.org/10.1146/annurev-matsci-062910-100448.

[21] O. Berger, The correlation between structure, multifunctional properties and applications of PVD MAX phase coatings. Part II. Texture and high-temperature properties, Surf. Eng. 36 (2020) 268–302, https://doi.org/10.1080/02670844.2019.1611076.

[22] Z. Zhang, X. Duan, D. Jia, Y. Zhou, S. van der Zwaag, On the formation mechanisms and properties of MAX phases: a review, J. Eur. Ceram. Soc. 41 (2021) 3851–3878, https://doi.org/10.1016/j.jeurceramsoc.2021.02.002.

[23] P. Eklund, J. Rosen, P.O.Å. Persson, Layered ternary $M_{n+1}AX_n$ phases and their 2D derivative MXene: an overview from a thin-film perspective, J. Phys. D Appl. Phys. 50 (2017) 113001, https://doi.org/10.1088/1361-6463/aa57bc.

[24] O. Berger, The correlation between structure, multifunctional properties and application of PVD MAX phase coatings. Part I. Texture and room temperature properties, Surf. Eng. 36 (2020) 225–267, https://doi.org/10.1080/02670844.2019.1611195.

[25] X. Li, X. Xie, J. Gonzalez-Julian, J. Malzbender, R. Yang, Mechanical and oxidation behavior of textured Ti_2AlC and Ti_3AlC_2 MAX phase materials, J. Eur. Ceram. Soc. 40 (2020) 5258–5271, https://doi.org/10.1016/j.jeurceramsoc.2020.07.043.

[26] E.N. Reshetnyak, A.S. Kuprin, T.A. Prikhna, M.A. Bortnitskaya, V.A. Belous, Synthesis, structure and protective properties of PVD MAX phase coatings. A review. Part I. MAX phase coatings deposition, Probl. Atom. Sci. Tech. (2023) 111–125, https://doi.org/10.46813/2023-147-11.

[27] M.W. Barsoum, T. El-Raghy, Room-temperature ductile carbides, Metall. Mater. Trans. A 30 (1999) 363–369, https://doi.org/10.1007/s11661-999-0325-0.

[28] N. Haddad, E. Garcia-Caurel, L. Hultman, M.W. Barsoum, G. Hug, Dielectric properties of Ti_2AlC and Ti_2AlN MAX phases: the conductivity anisotropy, J. Appl. Phys. 104 (2008) 023531, https://doi.org/10.1063/1.2960340.

[29] J.D. Hettinger, S.E. Lofland, P. Finkel, T. Meehan, J. Palma, K. Harrell, S. Gupta, A. Ganguly, T. El-Raghy, M.W. Barsoum, Electrical transport, thermal transport, and elastic properties of M_2AlC (M=Ti , Cr, Nb, and V), Phys. Rev. B 72 (2005) 115120, https://doi.org/10.1103/PhysRevB.72.115120.

[30] M. Xu, J. Yang, L. Liu, Temperature-dependent optical and electrical properties of bulk Ti_2AlC and two-dimensional MXenes from first-principles, Phys. B Condens. Matter 560 (2019) 146–154, https://doi.org/10.1016/j.physb.2019.02.025.

[31] J. Gertzen, P. Levecque, T. Rampai, T. van Heerden, DFT study of MAX phase surfaces for electrocatalyst support materials in hydrogen fuel cells, Materials 14 (2020) 77, https://doi.org/10.3390/ma14010077.

[32] Y. Bai, X. He, C. Zhu, G. Chen, Microstructures, electrical, thermal, and mechanical properties of bulk Ti_2AlC synthesized by self-propagating high-temperature combustion synthesis with pseudo hot isostatic pressing, J. Am. Ceram. Soc. 95 (2012) 358–364, https://doi.org/10.1111/j.1551-2916.2011.04934.x.

[33] M. Magnuson, M. Mattesini, Chemical bonding and electronic-structure in MAX phases as viewed by X-ray spectroscopy and density functional theory, Thin Solid Films 621 (2017) 108–130, https://doi.org/10.1016/j.tsf.2016.11.005.

[34] M.C. Guenette, M.D. Tucker, M. Ionescu, M. Bilek, D.R. McKenzie, Cathodic arc co-deposition of highly oriented hexagonal Ti and Ti_2AlC MAX phase thin films, Thin Solid Films 519 (2010) 766–769, https://doi.org/10.1016/j.tsf.2010.09.007.

[35] C. Torres, R. Quispe, N.Z. Calderón, L. Eggert, M. Hopfeld, C. Rojas, M.K. Camargo, A. Bund, P. Schaaf, R. Grieseler, Development of the phase composition and the properties of Ti_2AlC and Ti_3AlC_2 MAX-phase thin films – a multilayer approach towards high phase purity, Appl. Surf. Sci. 537 (2021) 147864, https://doi.org/10.1016/j.apsusc.2020.147864.

[36] D.J. Tallman, L. He, B.L. Garcia-Diaz, E.N. Hoffman, G. Kohse, R.L. Sindelar, M. W. Barsoum, Effect of neutron irradiation on defect evolution in Ti_3SiC_2 and Ti_2AlC, J. Nucl. Mater. 468 (2016) 194–206, https://doi.org/10.1016/j.jnucmat.2015.10.030.

[37] C. Ma, W. Yu, Y. Ma, G. Ma, H. Wang, Atomic level out-diffusion and interfacial reactions of MAX phases in contact with metals and air, J. Eur. Ceram. Soc. 44 (2024) 1–22, https://doi.org/10.1016/j.jeurceramsoc.2023.08.014.

[38] D.J. Tallman, B. Anasori, M.W. Barsoum, A critical review of the oxidation of Ti_2AlC, Ti_3AlC_2 and Cr_2AlC in air, Mater. Res. Lett. 1 (2013) 115–125, https://doi.org/10.1080/21663831.2013.806364.

[39] J. Frodelius, J. Lu, J. Jensen, D. Paul, L. Hultman, P. Eklund, Phase stability and initial low-temperature oxidation mechanism of Ti_2AlC thin films, J. Eur. Ceram. Soc. 33 (2013) 375–382, https://doi.org/10.1016/j.jeurceramsoc.2012.09.003.

[40] M. Haftani, M. Saeedi Heydari, H.R. Baharvandi, N. Ehsani, Studying the oxidation of Ti_2AlC MAX phase in atmosphere: a review, Int. J. Refract. Met. Hard Mater. 61 (2016) 51–60, https://doi.org/10.1016/j.ijrmhm.2016.07.006.

[41] Z. Zhang, D.M.Y. Lai, S.H. Lim, J. Chai, S. Wang, H. Jin, J. Pan, Isothermal oxidation of the Ti_2AlC MAX phase coatings deposited by kerosene-fuelled HVOF spray, Corros. Sci. 138 (2018) 266–274, https://doi.org/10.1016/j.corsci.2018.04.022.

[42] M. Sonestedt, J. Frodelius, M. Sundberg, L. Hultman, K. Stiller, Oxidation of Ti_2AlC bulk and spray deposited coatings, Corros. Sci. 52 (2010) 3955–3961, https://doi.org/10.1016/j.corsci.2010.08.004.

[43] S. Badie, A. Dash, Y.J. Sohn, R. Vaßen, O. Guillon, J. Gonzalez-Julian, Synthesis, sintering, and effect of surface roughness on oxidation of submicron Ti_2AlC ceramics, J. Am. Ceram. Soc. 104 (2021) 1669–1688, https://doi.org/10.1111/jace.17582.

[44] M. Guo, G. Cao, H. Pan, J. Guo, C. Chen, B. Zhang, J. Hu, Recent progress in synthesis of MAX phases and oxidation & corrosion mechanism: a review, Mater. Res. Lett. 12 (2024) 765–796, https://doi.org/10.1080/21663831.2024.2379567.

[45] P. Greil, Self-healing engineering ceramics with oxidation-induced crack repair, Adv. Eng. Mater. 22 (2020) 1901121, https://doi.org/10.1002/adem.201901121.

[46] B. Yao, S. Li, W. Zhang, W. Yu, Y. Zhou, S. Fan, G. Bei, Self-healing behavior of Ti_2AlC at a low oxygen partial pressure, J. Adv. Ceram. 11 (2022) 1687–1695, https://doi.org/10.1007/s40145-022-0640-0.

[47] F. Kong, K. Feng, Y. Bai, N. Li, X. Qi, Y. Zheng, R. Wang, X. He, Oxidation behavior of high-purity nonstoichiometric Ti_2AlC powders in flowing air, J. Mater. Res. 32 (2017) 2747–2754, https://doi.org/10.1557/jmr.2017.83.

[48] Z. Zhang, H. Jin, D.L. Mei Ying, J. Chai, S. Wang, J. Pan, Origin of anomalous laminar cracking, volume expansion and weight increase of Ti_2AlC MAX phase powders at 600 °C, Corros. Sci. 164 (2020) 108349, https://doi.org/10.1016/j.corsci.2019.108349.

[49] H. Zhu, X. Qian, H. Wu, J. Lei, Y. Song, X. He, Y. Zhou, Cyclic oxidation of ternary layered Ti_2AlC at 600–1000°C in air, Int. J. Appl. Ceram. Technol. 12 (2015) 403–410, https://doi.org/10.1111/ijac.12182.
[50] A. Donchev, M. Schütze, E. Ström, M. Galetz, Oxidation behaviour of the MAX-phases Ti_2AlC and $(Ti, Nb)_2AlC$ at elevated temperatures with and without fluorine treatment, J. Eur. Ceram. Soc. 39 (2019) 4595–4601, https://doi.org/10.1016/j.jeurceramsoc.2019.07.040.
[51] S. Badie, D. Sebold, R. Vaßen, O. Guillon, J. Gonzalez-Julian, Mechanism for breakaway oxidation of the Ti_2AlC MAX phase, Acta Mater. 215 (2021) 117025, https://doi.org/10.1016/j.actamat.2021.117025.
[52] L. Guo, G. Li, J. Wu, X. Wang, Effects of pellet surface roughness and pre-oxidation temperature on CMAS corrosion behavior of Ti_2AlC, J. Adv. Ceram. 11 (2022) 945–960, https://doi.org/10.1007/s40145-022-0588-0.
[53] N. Markocsan, D. Manitsas, J. Jiang, S. Björklund, MAX-phase coatings produced by thermal spraying, J. Superhard Mater. 39 (2017) 355–364, https://doi.org/10.3103/S1063457617050082.
[54] J. Frodelius, M. Sonestedt, S. Björklund, J.-P. Palmquist, K. Stiller, H. Högberg, L. Hultman, Ti_2AlC coatings deposited by high velocity oxy-fuel spraying, Surf. Coating. Technol. 202 (2008) 5976–5981, https://doi.org/10.1016/j.surfcoat.2008.06.184.
[55] S. Rech, A. Surpi, S. Vezzù, A. Patelli, A. Trentin, J. Glor, J. Frodelius, L. Hultman, P. Eklund, Cold-spray deposition of Ti_2AlC coatings, Vacuum 94 (2013) 69–73, https://doi.org/10.1016/j.vacuum.2013.01.023.
[56] A. Elsenberg, M. Busato, F. Gärtner, A. List, A. Bruera, G. Bolelli, L. Lusvarghi, T. Klassen, Influence of MAX-phase deformability on coating formation by cold spraying, J. Therm. Spray Technol. 30 (2021) 617–642, https://doi.org/10.1007/s11666-020-01110-w.
[57] H. Gutzmann, F. Gärtner, D. Höche, C. Blawert, T. Klassen, Cold spraying of Ti_2AlC MAX-phase coatings, J. Therm. Spray Technol. 22 (2013) 406–412, https://doi.org/10.1007/s11666-012-9843-1.
[58] A. Moridi, S.M. Hassani-Gangaraj, M. Guagliano, M. Dao, Cold spray coating: review of material systems and future perspectives, Surf. Eng. 30 (2014) 369–395, https://doi.org/10.1179/1743294414Y.0000000270.
[59] J. Akedo, Room temperature impact consolidation (RTIC) of fine ceramic powder by aerosol deposition method and applications to microdevices, J. Therm. Spray Technol. 17 (2008) 181–198, https://doi.org/10.1007/s11666-008-9163-7.
[60] J. Exner, M. Schubert, D. Hanft, J. Kita, R. Moos, How to treat powders for the room temperature aerosol deposition method to avoid porous, low strength ceramic films, J. Eur. Ceram. Soc. 39 (2019) 592–600, https://doi.org/10.1016/j.jeurceramsoc.2018.08.008.
[61] D. Hanft, J. Exner, M. Schubert, T. Stöcker, P. Fuierer, R. Moos, An overview of the aerosol deposition method: process fundamentals and new trends in materials applications, J. Ceram. Sci. Technol. 6 (2015) 147–182, https://doi.org/10.4416/JCST2015-00018.
[62] J. Adamczyk, P. Fuierer, Compressive stress in nano-crystalline titanium dioxide films by aerosol deposition, Surf. Coating. Technol. 350 (2018) 542–549, https://doi.org/10.1016/j.surfcoat.2018.07.015.
[63] J. Akedo, Room temperature impact consolidation and application to ceramic coatings: aerosol deposition method, J. Ceram. Soc. Japan 128 (2020) 101–116, https://doi.org/10.2109/jcersj2.19196.
[64] J. Kwon, H. Park, I. Lee, C. Lee, Effect of gas flow rate on deposition behavior of Fe-based amorphous alloys in vacuum kinetic spray process, Surf. Coating. Technol. 259 (2014) 585–593, https://doi.org/10.1016/j.surfcoat.2014.10.026.
[65] U. Eckstein, N.H. Khansur, D. Urushihara, T. Asaka, K. Kakimoto, T. Fey, K. G. Webber, Defect modulated dielectric properties in powder aerosol deposited ceramic thick films, Ceram. Int. 48 (2022) 33082–33091, https://doi.org/10.1016/j.ceramint.2022.07.241.
[66] A. Elsenberg, F. Gärtner, T. Klassen, Aerosol deposition of Ti_3SiC_2-MAX-Phase coatings, J. Therm. Spray Technol. 30 (2021) 1121–1135, https://doi.org/10.1007/s11666-021-01194-y.
[67] S.S. Manokhin, V.Y. Barinov, O.A. Golosova, Aerosol deposition of MAX phase-based coatings onto high-temperature nickel alloy, Int. J. Self-Propag. High-Temp. Synth. 28 (2019) 210–212, https://doi.org/10.3103/S1061386219030087.
[68] J. Henon, M.A. Piechowiak, O. Durand-Panteix, G. Etchegoyen, O. Masson, C. Dublanche-Tixier, P. Marchet, B. Lucas, F. Rossignol, Dense and highly textured coatings obtained by aerosol deposition method from Ti_3SiC_2 powder: comparison to a dense material sintered by spark plasma sintering, J. Eur. Ceram. Soc. 35 (2015) 1179–1189, https://doi.org/10.1016/j.jeurceramsoc.2014.10.012.
[69] M. Schubert, M. Hahn, J. Exner, J. Kita, R. Moos, Effect of substrate hardness and surface roughness on the film formation of aerosol-deposited ceramic films, Funct. Mater. Lett. 10 (2017) 1750045, https://doi.org/10.1142/S179360471750045X.
[70] C. Lee, M.-Y. Cho, M. Kim, J. Jang, Y. Oh, K. Oh, S. Kim, B. Park, B. Kim, S.-M. Koo, et al., Applicability of aerosol deposition process for flexible electronic device and determining the film formation mechanism with cushioning effects, Sci. Rep. 9 (2019) 2166, https://doi.org/10.1038/s41598-019-38477-y.
[71] B. Daneshian, F. Gärtner, H. Assadi, M.V. Vidaller, D. Höche, T. Klassen, Features of ceramic nanoparticle deformation in aerosol deposition explored by molecular dynamics simulation, Surf. Coating. Technol. 429 (2022) 127886, https://doi.org/10.1016/j.surfcoat.2021.127886.
[72] Y. Ichikawa, K. Shinoda, Current status and challenges for unified understanding of bonding mechanism in solid particle deposition process, Mater. Trans. 62 (2021) 691–702, https://doi.org/10.2320/matertrans.T-M2021813.
[73] D. Paulus, J. Kita, R. Moos, Relaxation behavior of intrinsic compressive stress in powder aerosol co-deposited films: rethinking PAD films as nanomaterials, Ceram. Int. 49 (2023) 38375–38381, https://doi.org/10.1016/j.ceramint.2023.09.065.
[74] J. Exner, T. Nazarenus, D. Hanft, J. Kita, R. Moos, What happens during thermal post-treatment of powder aerosol deposited functional ceramic films? Explanations based on an experiment-enhanced literature survey, Adv. Mater. 32 (2020) e1908104, https://doi.org/10.1002/adma.201908104.
[75] M. Schubert, N. Leupold, J. Exner, J. Kita, R. Moos, High-temperature electrical insulation behavior of alumina films prepared at room temperature by aerosol deposition and influence of annealing process and powder impurities, J. Therm. Spray Technol. 27 (2018) 870–879, https://doi.org/10.1007/s11666-018-0719-x.
[76] T. Nazarenus, K. Schlesier, F. Lebeda, M. Retsch, R. Moos, Microstrain release decouples electronic and thermal conductivity in powder aerosol deposited films, Mater. Lett. 322 (2022) 132461, https://doi.org/10.1016/j.matlet.2022.132461.
[77] M. Schubert, J. Exner, R. Moos, Influence of carrier gas composition on the stress of Al_2O_3 coatings prepared by the aerosol deposition method, Materials 7 (2014) 5633–5642, https://doi.org/10.3390/ma7085633.
[78] M.A. Piechowiak, J. Henon, O. Durand-Panteix, G. Etchegoyen, V. Coudert, P. Marchet, F. Rossignol, Growth of dense Ti_3SiC_2 MAX phase films elaborated at room temperature by aerosol deposition method, J. Eur. Ceram. Soc. 34 (2014) 1063–1072, https://doi.org/10.1016/j.jeurceramsoc.2013.11.019.
[79] T. Nazarenus, K. Schlesier, S. Biberger, J. Exner, J. Kita, A. Köhler, R. Moos, Posttreatment of powder aerosol deposited oxide ceramic films by high power LED, Int. J. Appl. Ceram. Technol. 19 (2022) 1540–1553, https://doi.org/10.1111/ijac.13977.
[80] H. Xue, P.-H. Huang, M. Göthelid, A. Strömberg, F. Niklaus, J. Li, Ultrahigh-rate on-paper PEDOT:PSS-Ti_2C microsupercapacitors with large areal capacitance, Adv. Funct. Mater. 34 (2024) 2409210, https://doi.org/10.1002/adfm.202409210.
[81] J. Exner, M. Hahn, M. Schubert, D. Hanft, P. Fuierer, R. Moos, Powder requirements for aerosol deposition of alumina films, Adv. Powder Technol. 26 (2015) 1143–1151, https://doi.org/10.1016/j.apt.2015.05.016.
[82] M.C. Guenette, M.D. Tucker, M. Ionescu, M.M.M. Bilek, D.R. McKenzie, Carbon diffusion in alumina from carbon and Ti_2AlC thin films, J. Appl. Phys. 109 (2011) 83503, https://doi.org/10.1063/1.3573490.
[83] D. Paulus, S. Bresch, R. Moos, D. Schönauer-Kamin, Powder aerosol deposited calcium cobaltite as textured P-type thermoelectric material with power factors approaching single crystal values, J. Eur. Ceram. Soc. 44 (2024) 116717, https://doi.org/10.1016/j.jeurceramsoc.2024.116717.
[84] J. Exner, P. Fuierer, R. Moos, Aerosol deposition of (Cu,Ti) substituted bismuth vanadate films, Thin Solid Films 573 (2014) 185–190, https://doi.org/10.1016/j.tsf.2014.11.037.
[85] Z. Zhang, S.H. Lim, D.M.Y. Lai, S.Y. Tan, X.Q. Koh, J. Chai, S.J. Wang, H. Jin, J. S. Pan, Probing the oxidation behavior of Ti_2AlC MAX phase powders between 200 and 1000 °C, J. Eur. Ceram. Soc. 37 (2017) 43–51, https://doi.org/10.1016/j.jeurceramsoc.2016.08.004.
[86] Z. Yan, L. Guo, Z. Zhang, X. Wang, F. Ye, Versatility of potential protective layer material Ti_2AlC on resisting CMAS corrosion to thermal barrier coatings, Corros. Sci. 167 (2020) 108532, https://doi.org/10.1016/j.corsci.2020.108532.
[87] M. Stumpf, T. Fey, P. Greil, Thermochemical calculations of the stability of Ti_2AlC in various atmospheres, J. Ceram. Sci. Technol. 7 (2016) 223–228, https://doi.org/10.4416/JCST2016-00029.
[88] R. Huang, G. Xu, C. Zhao, Q. Wu, L. Yu, C. Wu, The thermal stability of Ti_2AlC and Ag/Ti_2AlC in Ar and air, Mater. Char. 213 (2024) 114050, https://doi.org/10.1016/j.matchar.2024.114050.
[89] T. Scabarozi, A. Ganguly, J.D. Hettinger, S.E. Lofland, S. Amini, P. Finkel, T. El-Raghy, M.W. Barsoum, Electronic and thermal properties of $Ti_3Al(C_{0.5},N_{0.5})_2$, $Ti_2Al(C_{0.5},N_{0.5})$ and Ti_2AlN, J. Appl. Phys. 104 (2008) 073713, https://doi.org/10.1063/1.2979326.
[90] M. Mandegari, K. Nasouri, L. Ghasemi-Mobarakeh, Synthesis of low-cost Ti_3AlC_2-Ti_2AlC dual MAX phase with high-electrical conductivity using economical raw materials and novel compositions, Mater. Today Commun. 36 (2023) 106868, https://doi.org/10.1016/j.mtcomm.2023.106868.
[91] M.A. Pietzka, J.C. Schuster, Summary of constitutional data on the aluminum-carbon-titanium system, JPE 15 (1994) 392–400, https://doi.org/10.1007/BF02647559.
[92] M. Dahlqvist, B. Alling, I.A. Abrikosov, J. Rosén, Phase stability of Ti_2AlC upon oxygen incorporation: a first-principles investigation, Phys. Rev. B 81 (2010) 024111, https://doi.org/10.1103/PhysRevB.81.024111.
[93] T. Liao, J. Wang, Y. Zhou, First-principles investigation of intrinsic defects and (N, O) impurity atom stimulated Al vacancy in Ti_2AlC, Appl. Phys. Lett. 93 (2008) 261911, https://doi.org/10.1063/1.3058718.